Available online at www.sciencedirect.com
ScienceDirect
Journal of Nuclear Materials 362 (2007) 248–252
journal of nuclear materials
www.elsevier.com/locate/jnucmat

High temperature corrosion of a nickel base alloy by helium impurities

F. Rouillard [a,*], C. Cabet [b], K. Wolski [c], A. Terlain [b], M. Tabarant [d], M. Pijolat [e], F. Valdivieso [e]

[a] DPC/SCCME, CEA Saclay, Ecole Nationale Supérieure des Mines de St Etienne, France
[b] DEN/DANS/DPC/SCCME/LECNA, CEA Saclay, France
[c] Ecole Nationale Supérieure des Mines de St Etienne, Centre SMS/MPI, France
[d] DEN/DANS/DPC/SCP/LRSI, CEA Saclay, France
[e] Ecole Nationale Supérieure des Mines de St Etienne, Centre SPIN, France

Abstract

High temperature corrosion properties of Haynes 230 were investigated in a purposely-designed facility under a typical very high temperature reactor (VHTR) impure helium medium. The study was focused on the surface oxide scale formation and its stability at about 1223 K. The alloy developed a Mn/Cr rich oxide layer on its surface under impure helium at 1173 K. Nevertheless, a deleterious reaction destructing the chromium oxide was evidenced above a critical temperature, T_A. Reagents and products of this last reaction were investigated.

PACS: 68.37.−d; 68.47.Fg; 68.49.−h; 68.55.Nq

1. Introduction

Generally speaking, the high temperature resistance of Ni based Cr rich alloys is related to the formation of a dense and adherent chromia surface scale that 'protects' from further rapid corrosion. The likely environment in very high temperature reactors (VHTR), helium cooled nuclear systems, is however very specific. The helium coolant should contain traces of impurities typically H_2, H_2O, CO, and CH_4 in the 0.1–10 Pa range [1]. Because there is no molecular oxygen, the oxygen potential, set by the H_2O/H_2 ratio, is low for a significant local carbon potential, determined by thermodynamic as well as kinetic factors of gas–metal reactions [2,3]. Corrosion tests under VHTR atmospheres have demonstrated that chromium containing alloys, specifically Inconel 617 and Hastelloy X (22 wt%Cr), either form surface scale or suffer from bulk carburization and/or decarburization, depending on the gas chemistry, the alloy composition and the temperature [4]. The changes in the bulk carbon content and the associated structural transformations can notably degrade the material mechanical properties and must definitely be precluded [5]. The tested alloys usually develop chromium rich oxide scales

* Corresponding author. Tel.: +33 16 908 6866; fax: +33 16 908 1586.
E-mail address: fabien.rouillard@cea.fr (F. Rouillard).

0022-3115/$ - see front matter
doi:10.1016/j.jnucmat.2007.01.049

at intermediate temperatures. But above a critical temperature T_A (roughly 1173 K in most cases), the surface oxide suffers from a 'destructive' reaction and cannot provide any protection against corrosion any more. This reaction, called 'microclimate reaction' by Brenner and Graham [1] is considered as a co-operative interaction between the surface oxide and the internal carbon of the alloy [6,7], and occurs until either all the Cr rich oxide or all the accessible carbon is removed.

Ni–Cr–W alloys are claimed to present high creep strength, a good hot workability together with improved oxidation resistance. Recently developed Haynes 230 could be a promising candidate material for the high temperature structures in a VHTR. However, the corrosion resistance of Haynes 230 is unknown in the reactor specific environment.

The purpose of this work is to investigate the high temperature corrosion of the Haynes 230 alloy in typical VHTR conditions. Focus was made on the short term oxidation behaviour at 1173 K and on the destruction of the oxide scale in impure helium atmospheres at higher temperatures.

2. Experimental procedures

The chemical composition of the alloy is summarized in Table 1. This material was provided by Haynes International in the plate form and mill-annealed condition (plate annealed at 1503 K followed by rapid cooling). Specimens were machined as 25 mm × 12 mm × 2 mm coupons, polished down to 1 μm alumina powder and ultrasonically degreased in an acetone–ethanol mixture. The Haynes 230 specimens were tested in a quartz tube reactor housed in a high temperature furnace under flowing impure helium (0.7 ml s^{-1} cm^{-2} of sample; atmospheric pressure). Gas compositions were analyzed at the inlet and at the outlet of the test furnace by a gas phase chromatograph. The residual moisture level was monitored at the inlet by a capacitive hygrometer. Table 2 reports the experimental impurity contents. A blank test was carried out without any sample in order to verify that the tube and sample holder do not significantly react with the impurities, or influence the gas composition. Specimens were tested according to a two step thermal program:

Table 2
Impurity content in helium for $P_{tot} = 101\,325$ Pa

	H_2	CO	CH_4	H_2O
Partial pressure (Pa)	19.3 ± 0.4	4.9 ± 0.1	1.9 ± 0.04	0.16 ± 0.08

- First step: heating up to 1173 K at a rate of 1 K min^{-1} followed by 25 h at 1173 K in impure helium (see Table 2).
- Second step: heating up to 1253 K at a rate of 0.5 K min^{-1} followed by 20 h at 1253 K in impure helium (see Table 2).

Cooling down was slowly performed under pure helium. After the corrosion tests, the samples were weighed and characterized by X-ray diffraction (XRD) using a Panalytical X'pert MPD with Co-Kα excitation, glow discharge optical emission spectroscopy (GDOES) using a Jobin-Yvon 50 model, field emission scanning electron microscopy (FESEM) using a LEO 1525 model, energy dispersive X-ray spectroscopy (EDXS) and microprobe (WDS) using a CAMECA SX 50 model.

3. Results and discussion

3.1. Oxidation in impure He at 1173 K

Structural analysis of the oxide scale: after the first step (1173 K, 25 h) in impure helium, the samples had a mean mass gain equal to 0.12 mg cm^{-2}. No spalling off was ever observed for any specimen. Fig. 1 is a field emission scanning electron microscopy picture of the sample surface after step 1. A continuous scale about 1 μm thick has grown. Low angle XRD analysis at 1° identified a spinel phase $Mn_{1.5}Cr_{1.5}O_4$ as well as Cr_2O_3. A linescan through this oxide layer by microprobe (WDS), also confirmed by a GDOES analysis, showed that the Mn-rich spinel was in the upper part of the scale whereas the Cr_2O_3 was mostly at the oxide/alloy interface. The GDOES analysis revealed, as well,

Table 1
Chemical composition of Haynes 230 [10]

Element	Ni	W	Cr	Mn	Fe	Ti	Si	Al	Mo	Co	C
Mass fraction (%)	59.6	14.7	22.0	0.5	1.3	0.1	0.4	0.4	1.3	0.2	0.105

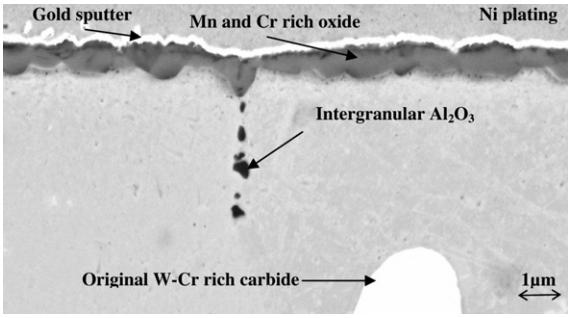

Fig. 1. FESEM picture at 20 keV with a BSE contrast; Haynes 230 surface after step 1 under impure helium.

inclusions of aluminium rich and silicon rich oxides at the oxide/alloy interface. Al distribution map obtained by EDXS indicated that this Al rich layer was not continuous and that some Al oxidized also along grain boundaries up to 10 μm deep inside the alloy.

Gas phase analysis during oxidation: gas phase chromatography analysis demonstrated that the carbon monoxide partial pressure in helium decreased, by increasing the temperature up to 1173 K under the helium mixture (Fig. 2). The CO uptake, then, stopped while maintaining the specimens at 1173 K for 25 h. This CO consumption can be attributed to the oxidation of metals by CO:

$$xM + yCO_{(gas)} \rightarrow M_xO_y + yC_{(sol)} \quad (1)$$

with M = Al, Cr, Mn, Si and $C_{(sol)}$ the carbon in solution in the alloy.

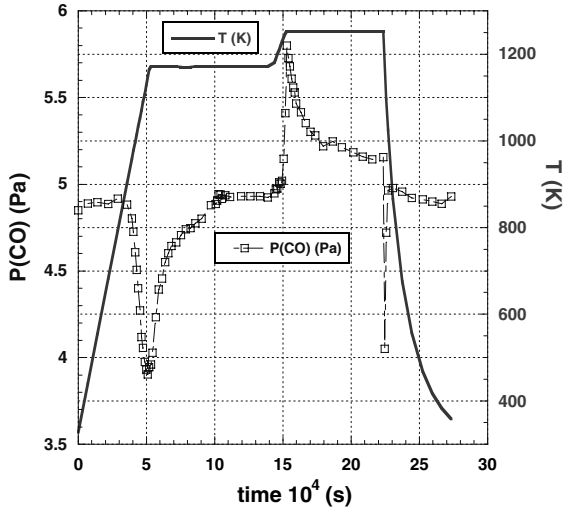

Fig. 2. Evolution of the CO content and temperature program as a function of time.

This reaction produced free carbon. Since neither metallic carbides nor carbon deposit was ever identified on the surface, elemental carbon should have diffused deeper in the alloy to react with any strong carbide-forming element (as Cr, W, Mo, etc.) (Fig. 5). An important observation is that carbon monoxide did not react with samples for ever (Fig. 2). Taking into account the strong hypothesis that CO reacts at the oxide/alloy interface as mentioned by previous studies [8,9], several reasons may explain this slowing down of CO surface reactivity:

(1) The surface oxide growth depletes the oxidable elements at the oxide/alloy interface. As a consequence, the activity of reagents in reaction (1) decreases.
(2) The slow diffusion of carbon away from the interface induces an accumulation which impedes reaction (1).
(3) Change in oxide porosity that becomes progressively more gas tight prevents CO from accessing to the oxide/alloy interface in order to react with alloying elements.

More experiments are needed to discriminate the rate-limiting process.

3.2. Destruction of the oxide layer

Gas phase analysis: gas phase analysis, during the second step (heating to 1253 K and maintaining for 20 h), showed a sharp release of CO reaching 0.9 Pa and starting at roughly 1243 ± 5 K (Fig. 2). This production, then, died away while the specimen temperature was maintained at 1253 K for 20 h.

Structural analysis of the surface: when the specimens were removed after step 2, no spalling off was observed. However, the mean mass gain was 0.06 mg cm^{-2} only, which is twice lower than after step 1. The alloy is likely to have lost weight during this next step. Fig. 3 shows a continuous oxide film on Haynes 230. This layer is thinner than after the oxidation test (Fig. 1). Linescans by microprobe and by GDOES (Fig. 4) showed that the surface oxide was depleted in chromium when compared to the oxide developed after step 1. On the opposite the alloy under the scale appeared to have been slightly enriched in chromium. Manganese was still detected in the oxide layer after step 2. In addition, the small nodules visible in Fig. 3 were analyzed as internal Al_2O_3 inclusions by EDXS-TEM.

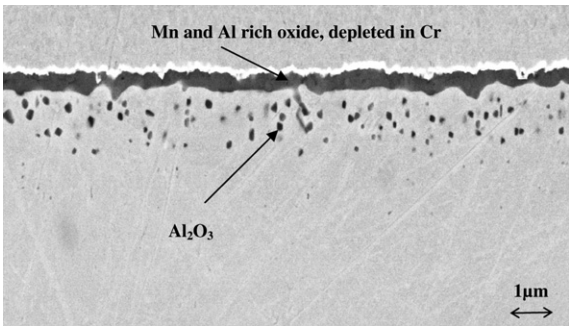

Fig. 3. FESEM picture at 20 keV with a BSE contrast; Haynes 230 surface after step 1 (1173 K, 25 h) and step 2 (1253 K, 20 h) under impure helium.

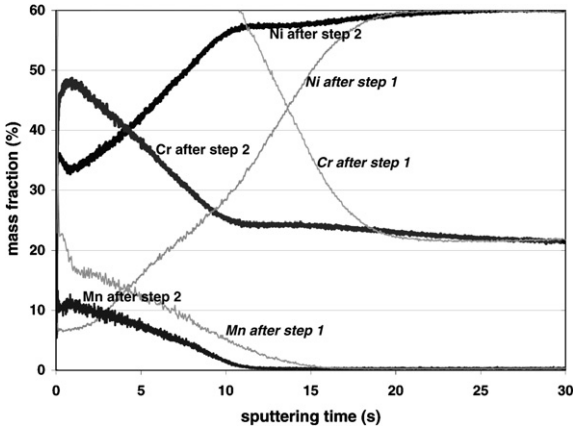

Fig. 4. GDOES profiles of Ni, Cr, Mn at the alloy surface after step 1 (1173 K, 25 h) and step 2 (1253 K, 20 h); oxide scale is on the left hand side and alloy bulk on the right hand side.

Because impurity/metal reactions cannot entirely explain the significant CO production (Fig. 2), another reaction has been proposed [1,6]: surface oxide and carbon contained in the alloy – as metallic carbides or as a dissolved element – have been suggested to react together according to Reaction (2):

$$Cr_2O_3 + 3C_{(sol)} \rightarrow 2Cr + 3CO_{(gas)} \quad (2)$$

From a thermodynamical point of view and depending on the activity of the different elements, chromium oxide and, to a smaller extent Mn and Si rich oxide, are the only oxides ready to be reduced by carbon at the given temperature. Al rich oxide cannot react at this temperature. The smaller mass gains after step 2, together with the thinner surface layer, confirm that the oxide scale has been partly removed. Besides, GDOES examinations imply that mostly Cr underwent reaction (2). Complementary GDOES analyzes were performed in order to clarify

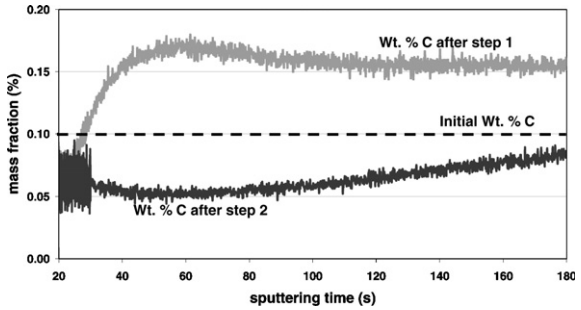

Fig. 5. GDOES profile of the carbon content at the alloy surface after step 1 (1173 K, 25 h) and step 2 (1253 K, 20 h); surface is on the left hand side and alloy bulk on the right hand side.

the role of carbon. Haynes 230 specimens that had been exposed in impure helium without methane (same composition as in Table 2 but the CH_4) were characterized after step 1 and after step 2. Fig. 5 shows that the destruction of the oxide layer went with a depletion of carbon beneath the scale that had likely diffused from matrix to the scale/alloy interface to react according to Eq. (2).

4. Conclusion

Haynes 230 corrosion by impurities in helium exhibited two specific regimes: either the oxide formation at $T < T_A$ or the oxide destruction at $T > T_A$. Oxidation of Haynes 230 under impure helium at 1173 K formed a mixed (Mn, Cr) spinel oxide and Cr_2O_3 on the alloy surface. Whereas carbon monoxide took part in the oxide formation at the initial time, as suggested by GDOES and GPC results, it appeared that water vapour was the main oxidant for longer times. Above the critical temperature T_A, the surface layer, developed in the first stage, anticipated its destruction by reacting with the carbon from the alloy. These analyzes showed that chromium is the most reactive metal element of the oxide scale while manganese seemed, at least in a first stage, to remain in the surface layer.

Because the long term resistance of Haynes 230 relies on the growth of a protective surface scale, the reduction of the pre-formed oxide layer by its own carbon above a given temperature T_A represents a major risk for the material integrity. VHTR operations must, definitely, avoid that the alloy surface reaches T_A (including a significant safety margin). More studies are underway on the influence of the gas phase composition on this destructive reaction, especially on the role of the carbon monoxide and methane partial pressures in helium.

Acknowledgements

The authors are thankful to Mrs M.C. Lafont for performing TEM analyses at the Université Paul Sabatier of Toulouse and to Mr P. Bonnaillie for the FESEM pictures performed at the CEA/DEN/DANS/DMN/SRMP.

References

[1] K.G.E. Brenner, L.W. Graham, Nucl. Technol. 66 (1983) 404.
[2] W.J. Quadakkers, H. Schuster, Werstoffe und Korrosion 36 (1985) 141.
[3] W.J. Quadakkers, Mater. Sci. Eng. 87 (1986) 107.
[4] W.J. Quadakkers, Werstoffe und Korrosion 36 (1985) 335.
[5] Y. Hosoi, S. Abe, Metall. Trans. A 6 (1975) 1171.
[6] M.R. Warren, High Temp. Technol. 4 (1986) 119.
[7] H.J. Christ, U. Künecke, K. Meyer, H.G. Sockel, Mater. Sci. Eng. A 87 (1987) 161.
[8] I. Wolf, H.J. Grabke, P. Schmidt, Oxid. Met. 29 (1988) 289.
[9] K.G. Zheng, D.J. Young, Oxid. Met. 42 (1994) 163.
[10] Klarstrom, Mater. Design Approaches Exp. (2001) 297.